ChemComm

Ultra-small Mo-Pt subnanoparticles enable CO2 hydrogenation at room temperature and atmospheric pressure

Journal:	*ChemComm*
Manuscript ID	CC-COM-06-2023-002703.R2
Article Type:	Communication

COMMUNICATION

Ultra-small Mo-Pt subnanoparticles enable CO_2 hydrogenation at room temperature and atmospheric pressure

Received 00th January 20xx,
Accepted 00th January 20xx

DOI: 10.1039/x0xx00000x

Augie Atqa,[a] Masataka Yoshida,[a] Masanori Wakizaka,[c] Wang-Jae Chun,[d] Akira Oda,[e] Takane Imaoka *[a,b] and Kimihisa Yamamoto *[a,b]

We present a partially-oxidised bimetallic Mo-Pt subnanoparticle ($Mo_4Pt_8O_x$) enabling thermally-driven CO_2 hydrogenation to CO at room temperature and atmospheric pressure. A mechanistic study explained the full catalytic cycle of the reaction from CO_2 activation to catalyst reactivation. DFT calculations revealed that alloying with Mo lowers the activation barrier by weakening the CO adsorption. This finding could be a first step for low-energy CO_2 conversion.

Subnanometer metal particles, composed of a few to tens of atoms, possess distinct coordination structures featuring discrete electronic levels and deficient coordination numbers.[1] This characteristic gives them exceptionally high reactivity, which is not observed in bulk metals or nanoparticles. For example, platinum subnanoparticles have demonstrated excellent catalytic activity for the oxygen reduction reaction (ORR) due to their surface structures, which differ entirely from those of bulk and nanoparticle counterparts with an FCC (face-centred-cubic) structure.[2,3] Likewise, copper subnanoparticles have exhibited high catalytic activity in the aerobic oxidation of toluene due to the increased ionicity of the Cu-O bonds on the catalyst surface resulting from their unique structure.[4,5] Subnanoparticles also display intrinsic atomic dynamics not found in crystalline nanoparticles, and it has been suggested that these dynamics is the source of their high reactivity.[6,7]

Another characteristic of subnanoparticles is that they are free of phase separation. Unlike nanoparticles, subnanoparticle achieves a homogeneous mixture of five noble and typical metals.[8] This characteristic results in a significantly enhanced synergistic effect between the elements, making them a group of materials with significant advantages as catalysts.[9] These unique properties make subnanoparticles a promising candidate for materials that allow thermally-driven catalytic CO_2 conversion at room temperature. Contrary to these expectations, however, there have yet to be studies of subnanoparticles as catalysts for CO_2 reduction.

We have designed a new bimetallic Mo-Pt subnanoparticle based on the recent discovery that Mo subnanoparticles tend to form an amorphous oxycarbide structure[10], making them effective as selective hydrogenation catalysts for CO_2.[11] The present subnanoparticle's composition hybridises Mo and Pt at the atomic level, combining their respective active sites for CO_2 and H_2 decomposition. Here, we demonstrate the successful development of an ultra-small $Mo_4Pt_8O_x$ subnanoparticle that catalyses the hydrogenation of CO_2 to CO at atmospheric pressure from room temperature.

Metal and alloy subnanoparticles employed in this study were prepared using a dendrimer-based template. A phenyl-azomethine dendrimer has a rigid structure with an intramolecular potential gradient, enabling precise control and a diverse multi-metallic combination of the atomic composition.[12] After conducting the precise complexation of dendrimer and metal ions, the complexes were immobilised to TiO_2, followed by the thermal hydrogen reduction at 500 °C for 30 min. As a reference, a nanoparticle sample with the same elemental composition was prepared by sintering the as-synthesised subnanoparticle at 600 °C for 3 h under the Ar atmosphere (**Fig. S1**).

The subnanoparticles supported on TiO_2 were identified by electron microscopy and X-ray analysis. The high-resolution scanning transmission electron microscopy (HAADF-STEM) observation revealed that the particle size of the synthesised bimetallic $Mo_4Pt_8O_x$ subnanoparticle supported on TiO_2 was

[a] *Institute of Innovative Research, Tokyo Institute of Technology, Yokohama 226-8503, Japan.*
[b] *JST ERATO Yamamoto Atom Hybrid Project, Tokyo Institute of Technology, Yokohama 226-8503, Japan.*
[c] *Graduate School of Photonics Science, Chitose Institute of Science and Technology, Chitose 066-0012, Japan.*
[d] *Graduate School of Arts and Sciences, International Christian University, Tokyo 181-8585, Japan.*
[e] *Graduate School of Engineering, Nagoya University, Nagoya 464-8603, Japan.*
E-mails: yamamoto@res.titech.ac.jp (K.Y.), timaoka@res.titech.ac.jp (T.I.)
Electronic Supplementary Information (ESI) available: [details of any supplementary information available should be included here]. See DOI: 10.1039/x0xx00000x

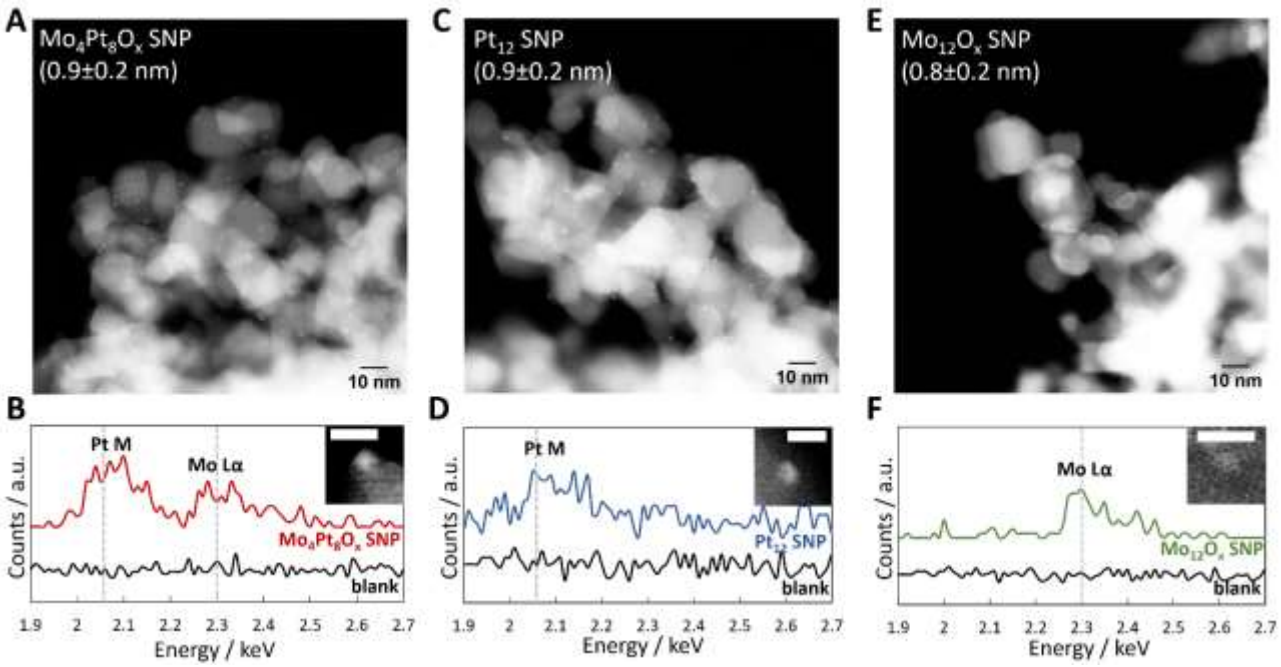

Fig. 1 HAADF-STEM observation and ultra-small EDS analysis of the $Mo_4Pt_8O_x$ (**A**, **B**), Pt_{12} (**C**, **D**), and $Mo_{12}O_x$ (**E**, **F**) subnanoparticles supported on TiO_2 (scale bar on **B**, **D**, **F**: 2 nm).

0.9±0.2 nm. The ultra-small EDS measurement of one particle region (ca. 3 nm × 3 nm) showed the coexistence of Mo and Pt atoms inside the 1-nm-sized $Mo_4Pt_8O_x$ subnanoparticle, indicating that Mo and Pt alloying was achieved at the subnano-scale (**Fig. 1A, B**), with Mo-Pt ratio 1/(2.1±0.2) from more than 30 EDS samples (**Fig. S2**). The syntheses of monometallic Pt_{12} and $Mo_{12}O_x$ on TiO_2 were also confirmed (**Fig. 1C, D, E, F**). The electronic properties of as-synthesised subnanoparticles were analysed using X-ray photoelectron spectroscopy (XPS). The $Pt4f_{7/2}$ binding energies of $Mo_4Pt_8O_x/TiO_2$ and Pt_{12}/TiO_2 were 71.9 and 72.0 eV, respectively, indicating Pt^0 at the subnano scale (**Fig. S3A**).[2] On the other hand, the $Mo3d_{5/2}$ binding energies of $Mo_4Pt_8O_x/TiO_2$ and $Mo_{12}O_x/TiO_2$ were 229.1 ($Mo^{\sim 4+}$) and 229.7 eV ($Mo^{4+\sim 6+}$), respectively (**Fig. S3B**). These electronic states were also supported by X-ray absorption near edge structure (XANES) (**Fig. S3C, D, E**). Alloying Mo with Pt further reduced the Mo species to ~4+.

Catalytic performances of subnanoparticles on CO_2 hydrogenation at atmospheric pressure (1 bar) were evaluated between room temperature and 150 °C (**Fig. 2A**). Before each experiment, a pre-treatment of the subnanoparticle was carried out under H_2 gas flow (20 ml/min) at 150°C for 1 hour. A continuous flow reactor was used to evaluate catalytic performances with the mixed gas flow: CO_2 10 ml/min, H_2 10 ml/min. We defined $T_{CO2\ to\ CO}$ as the temperature at which CO_2 hydrogenation starts if the CO production rate exceeds 1 μmol g_{cat}^{-1} h^{-1}. Whereas $Mo_{12}O_x/TiO_2$ showed no carbon monoxide (CO) product in this low-temperature region ($T_{CO2\ to\ CO}$ ($Mo_{12}O_x/TiO_2$) = 200°C, **Fig. S4**), Pt_{12}/TiO_2 showed CO production beginning from 40 °C. Even more surprising, $Mo_4Pt_8O_x/TiO_2$ starts the CO_2 hydrogenation catalysis from room temperature (**Fig. 2B**) with a CO production rate of 2.0±0.2 μmol g_{cat}^{-1} h^{-1} (500±50 μmol $g_{Mo\text{-}Pt\ atom}^{-1}$ h^{-1}) at 25°C. The catalytic activity at room temperature and atmospheric pressure was confirmed for 49 h (**Fig. 2C**). The particle size remains unchanged (0.9±0.2 nm) after the reaction. The decrease of the CO rate after 24 h

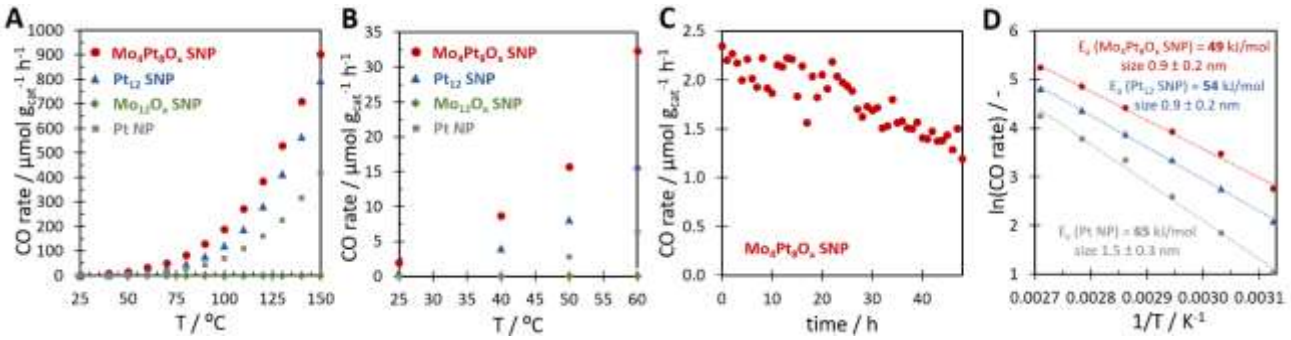

Fig. 2 Low-temperature CO_2 hydrogenation to CO over $Mo_4Pt_8O_x$ (0.4 wt.%, red circle), Pt_{12} (0.4 wt.%, blue triangle), $Mo_{12}O_x$ (0.4 wt.%, green diamond) subnanoparticles, and Pt nanoparticles (0.4 wt.%, grey square) supported on TiO_2 at 1 bar, RT-150 °C, 150 mg catalyst each, CO_2 10 ml/min, H_2 10 ml/min, hold time 30 min each temperature (**A**, **B**). Time-course CO_2 hydrogenation to CO at room temperature and atmospheric pressure using $Mo_4Pt_8O_x$ subnanoparticles (150 mg, CO_2 10 ml/min, H_2 10 ml/min) (**C**). Arrhenius plot of the reaction over $Mo_4Pt_8O_x$, Pt_{12} subnanoparticles, and Pt nanoparticles supported on TiO_2 (**D**).

was possibly due to the adsorption of generated H_2O on the catalyst surface (**Fig. S5**). No methane production was detected in the reaction employing $Mo_4Pt_8O_x/TiO_2$ and Pt_{12}/TiO_2 subnanoparticles. It is the same trend as the previous reports, which employed smaller metal nanoparticle catalysts that selectively produce CO than CH_4.[13,14] Four blank experiments were performed to ensure that the detected CO is from the CO_2 hydrogenation: (1) CO_2 and H_2 without the catalyst, (2) CO_2 and H_2 with TiO_2, (3) CO_2 with the catalyst, and (4) H_2 with the catalyst. No production by entries (3) and (4) confirmed that the CO is not from the catalyst's organic residues (dendrimers). All the blank experiments showed no CO detection; thus, it was clearly demonstrated that $Mo_4Pt_8O_x/TiO_2$ catalysed the process, and CO formed was from CO_2. As a reference, the as-synthesised Pt/TiO_2 nanoparticle (1.5 ± 0.3 nm, **Fig. S1**) was also evaluated. It is inferior to the Pt_{12}/TiO_2 subnanoparticle and starts the CO_2 hydrogenation catalysis from 50 °C.

The higher catalytic activity of bimetallic $Mo_4Pt_8O_x/TiO_2$ subnanoparticle than that of monometallic Pt_{12}/TiO_2 subnanoparticles and Pt/TiO_2 nanoparticles is mainly due to the lower activation energy. The Arrhenius plots give the apparent activation energies of $Mo_4Pt_8O_x/TiO_2$, Pt_{12}/TiO_2 subnano-particles, and Pt/TiO_2 nanoparticles were 49, 54, and 65 kJ/mol, respectively (**Fig. 2D**). The results showed that the miniaturisation of Pt nanoparticles down to the subnanometer regime lowers the activation energy; moreover, alloying it with Mo further reduces the activation energy.

A proposed mechanism of room-temperature CO_2 hydrogenation over the $Mo_4Pt_8O_x/TiO_2$ subnanoparticle is shown in **Scheme 1**. First, CO_2 is activated on the $Mo_4Pt_8O_x/TiO_2$ subnanoparticle (ii). CO_2 is split into O and CO, where O oxidises the Mo species (One of the possibilities: Mo^{4+} to Mo^{6+}), and CO binds with the Pt atom, as shown in (iii). The former was supported by the results of *in situ* XANES measurement. *In situ* Mo K-edge XANES measurement revealed that upon the CO_2 introduction, the Mo K-edge energy significantly shifted to higher energy by 1 eV, indicating the oxidation of Mo species at room temperature (**Fig. 3A**). From linear interpolation analysis, the average Mo states changed from 4+ to 4.5+, suggesting the activation of CO_2 molecules by Mo species at room temperature. Notably, Pt electronic states did not change upon the CO_2 introduction (**Fig. S6**). The latter was supported by the *in situ* diffused reflectance infrared Fourier transform spectroscopy (DRIFTS) measurement. The *in situ* DRIFTS revealed that the CO vibration band for the CO species adsorbed on the Pt surface ($\nu CO_{(ad)}$, 2069 cm^{-1})[15-17] appeared upon the CO_2 introduction at room temperature (**Fig. 3B**). By purging with Ar gas for 30 min, the $\nu CO_{(ad)}$ intensity decreased, indicating the desorption of CO. The band further decreased by introducing H_2 for 30 min, suggesting that H_2 adsorbs on Pt surface, pushing away the CO molecules. The adsorbed H atoms react with the oxygen of Mo^{6+} to form H_2O (**Fig. S7**) and reactivate the catalyst (i) as the Mo-K spectrum returns to its original position. The full cycle of thermally-driven CO_2 hydrogenation to CO at 25°C and 1 bar was demonstrated and proven spectroscopically for the first time. It is worth noting that this catalytic process has been performed 3 cycles (**Fig.3A inset**).

Scheme 1 Proposed mechanism of room-temperature thermally-driven CO_2 hydrogenation to CO over $Mo_4Pt_8O_x$ subnanoparticles.

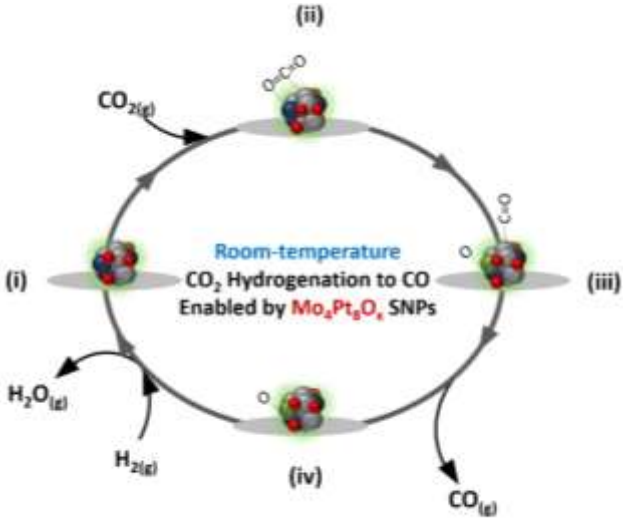

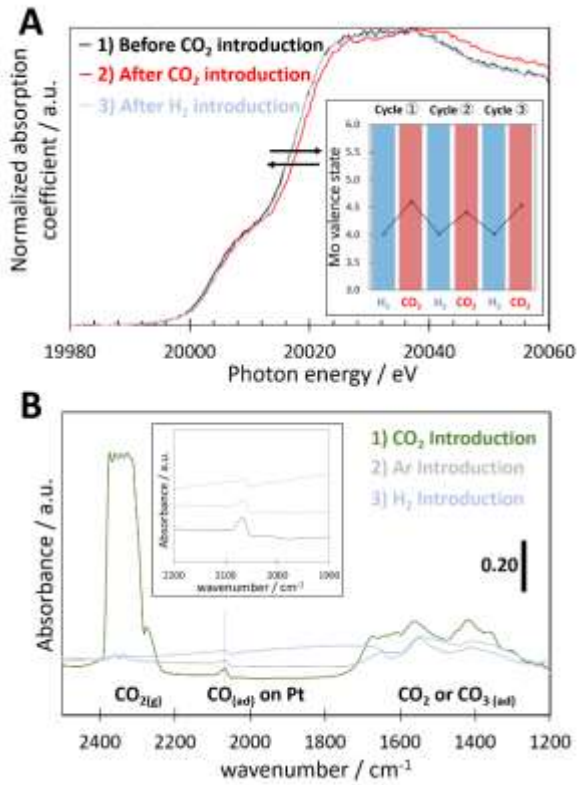

Fig. 3 *In situ* Mo K-edge XANES spectra of $Mo_4Pt_8O_x$ subnanoparticles at room temperature and atmospheric pressure 1) before CO_2 introduction, 2) after CO_2 introduction, and 3) after H_2 introduction (**A**). The inset shows three catalytic cycles of room-temperature CO_2 hydrogenation to CO. *In situ* DRIFTS spectra of $Mo_4Pt_8O_x$ subnanoparticles at room temperature after the introduction of 1) CO_2, 2) Ar, and 3) H_2 gas (**B**).

Concerning the proposed mechanism, the weakening CO adsorption energy is a possible reason for the lower activation energy of $Mo_4Pt_8O_x$ over the Pt_{12} subnanoparticle. *In situ* DRIFTS analyses revealed that CO readily formed upon the CO_2 introduction (ii to iii) at room temperature for both $Mo_4Pt_8O_x/TiO_2$ and Pt_{12}/TiO_2 (**Fig. S8B, D**). After introducing H_2,

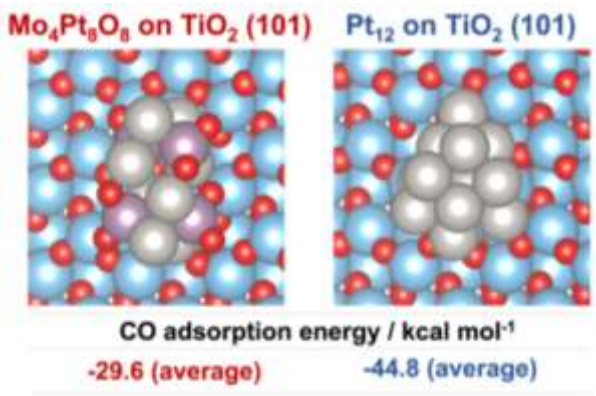

Fig. 4 DFT calculation results of Pt-CO adsorption energies on $Mo_4Pt_8O_8/TiO_2(101)$ and $Pt_{12}/TiO_2(101)$ models (Mo: purple, Pt: silver, O: red, Ti: blue).

the $\nu CO_{(ad)}$ on $Mo_4Pt_8O_x/TiO_2$ almost vanished, suggesting the completion of a catalytic cycle of CO_2 hydrogenation over the $Mo_4Pt_8O_x/TiO_2$ subnanoparticle. However, the $\nu CO_{(ad)}$ remained on Pt_{12}/TiO_2, indicating slow CO desorption. The difference in the CO desorption rate between $Mo_4Pt_8O_x/TiO_2$ and Pt_{12}/TiO_2 is the possible reason the CO production rate for Pt_{12}/TiO_2 did not exceed 1 μmol g_{cat}^{-1} h^{-1} at room temperature. The DFT calculations supported these analyses by performing the Pt-CO adsorption energy calculations for both $Mo_4Pt_8O_x$ and Pt_{12} on TiO_2. For the calculation model, we used $Mo_4Pt_8O_8$ as a model because of its $Mo^{\sim 4+}$ valence states from experimental results. It showed that alloying Pt with Mo significantly weakened the Pt-CO adsorption energy from -44.8 kcal/mol (average Pt-CO adsorption energy in $Pt_{12}/TiO_2(101)$) to -29.6 kcal/mol (average Pt-CO adsorption energy in $Mo_4Pt_8O_8/TiO_2(101)$, **Fig. 4, S9-S10**). These calculation results support the idea that the desorption of CO from $Mo_4Pt_8O_x/TiO_2$ is easier than that from Pt_{12}/TiO_2.

In summary, we have demonstrated thermally-driven CO_2 hydrogenation to CO using the $Mo_4Pt_8O_x$ subnanoparticle at room temperature and atmospheric pressure for the first time. Although several studies successfully activated and split CO_2 into CO and O (oxygen atom) at room temperature using oxygen-deficient solid-state materials such as electrides[18-21], realising the catalytic process has remained problematic because removing the split O from the material surface is difficult. In contrast, the present $Mo_4Pt_8O_x$ subnanoparticle enables oxygen removal at room temperature and atmospheric pressure, unlocking the first stage for low-energy CO_2 conversion to fuel.[22] *In situ* Mo K-edge XANES and DRIFTS analyses showed that the Mo-Pt combination promotes the activation of CO_2 and conversion to CO at 25°C and 1 bar. *In situ* DRIFTS analyses and DFT calculations revealed the excellent catalytic activity of $Mo_4Pt_8O_x/TiO_2$ subnanoparticles compared to Pt_{12}/TiO_2 subnanoparticles on room-temperature CO_2 hydrogenation to CO is due to the weakening CO adsorption energy.

This study was partly supported by JST ERATO Grant Number JPMJER1503, Japan (K.Y.), JSPS KAKENHI Grant Numbers JP 21H05023, 21H04684 (K.Y.), JP 22H05044, 22H02091, 22H05043 (T.I.), JP 22K14563(M.Y.), JST SPRING Grant Number JPMJSP2106 (A.A.). XAFS were conducted at BL9C and NW10A beamlines of the High Energy Accelerator Research Organization — Institute of Materials Structure Science—Photon Factory (KEK-IMSS-PF) under the approval of the Photon Factory Advisory Committee (No. 2021G688(T.I.) & 2023G054(A.A.)). The numerical calculations were carried out on the TSUBAME3.0 supercomputer at the Tokyo Institute of Technology, supported by the MEXT project of the Tokyo Tech Academy for Convergence of Materials and Informatics (TAC-MI). We thank Ms Y. Hayashi (Tokyo Institute of Technology) for assistance with the high-resolution STEM observations and Suzukakedai Materials Analysis Division (Tokyo Institute of Technology) for support with ICP-AES measurements.

Conflicts of interest

The authors declare no competing financial interest.

References

1 T. Imaoka, A. Kuzume, M. Tanabe, T. Tsukamoto, T. Kambe and K. Yamamoto, *Coord. Chem. Rev.*, 2023, **474**, 214826.
2 T. Imaoka, H. Kitazawa, W. -J. Chun and K. Yamamoto, *Angew. Chem. Int. Ed.*, 2015, **54 (34)**, 9810-9815.
3 K. Yamamoto, T. Imaoka, W. -J. Chun, O. Enoki, H. Katoh, M. Takenaga and A. Sonoi, *Nat. Chem.*, 2009, **1**, 397-402.
4 K. Sonobe, M. Tanabe and K. Yamamoto, *ACS Nano*, 2020, **14(2)**, 1804-1810.
5 K. Sonobe, M. Tanabe, T. Imaoka, W. -J. Chun and K. Yamamoto, *Chem. Eur. J.*, 2021, **27(33)**, 8452-8456.
6 Z. Zhang, B. Zandkarimi and A. N. Alexandrova, *Acc. Chem. Res.*, 2020, **53(2)**, 447-458.
7 B. Zandkarimi and A. N. Alexandrova, *J. Phys. Chem. Lett.*, 2019, **10(3)**, 460-467.
8 T. Tsukamoto, T. Kambe, A. Nakao, T. Imaoka and K. Yamamoto, *Nat. Commun.*, 2018, **9**, 3873.
9 Q. Zou, Y. Akada, A. Kuzume, M. Yoshida, T. Imaoka and K. Yamamoto, *Angew. Chem. Int. Ed.*, 2022, **61(40)**, e202209675.
10 M. Wakizaka, A. Atqa, W. -J. Chun, T. Imaoka, and K. Yamamoto, *Nanoscale*, 2020, **12**, 15814-15822.
11 M. Wakizaka, T. Imaoka and K. Yamamoto, *Small*, 2021, **17(19)**, 2008127.
12 K. Yamamoto, M. Higuchi, S. Shiki, M. Tsuruta and H. Chiba, *Nature*, 2002, **415**, 509-511.
13 Z. Zhao, M. Wang, P. Ma, Y. Zheng, J. Chen, H. Li, X. Zhang, K. Zheng, Q. Kuang and Z. -X. Xie, *Appl. Catal. B: Environ.*, 2021, **291**, 120101.
14 S. Mine, T. Yamaguchi, K. W. Ting, Z. Maeno, S. M. A. H. Siddiki, K. Oshima, S. Satokawa, K. Shimizu and T. Toyao, *Cat. Sci. Technol.*, 2021, **11**, 4172-4180.
15 B. Han, Y. Guo, Y. Huang, W. Xi, J. Xu, J. Luo, H. Qi, Y. Ren, X. Liu, B. Qiao and T. Zhang, *Angew. Chem. Int. Ed.*, 2020, **59(29)**, 11824-11829.
16 L. DeRita, S. Dai, K. Lopez-Zepeda, N. Pham, G. W. Graham, X. Pan and P. Christopher, *J. Am. Chem. Soc.*, 2017, **139(40)**, 14150-14165.
17 K. Ding, A. Gulec, A. M. Johnson, N. M. Schweitzer, G. D. Stucky, L. D. Marks and P. C. Stair, *Science*, 2015, **350(6257)**, 189-192.
18 Y. Sun, Y. Chen, X. Zhang, Y. He, Z. Qiu, W. Zheng, F. Wang, H. Jiao, Y. Yang, Y. Li and X. Wen, *Angew. Chem. Int. Ed.*, 2021, **60(48)**, 25538-25545.
19 D. Nagaraju, S. Gupta, D. Kumar, C. P. Jijil, S. K. Bhat, D. Jagadeesan and S. Ogale, *ACS Omega* 2017, **2(11)**, 8407-8413.
20 Y. Toda, H. Hirayama, N. Kuganathan, A. Torrisi, P. V. Sushko and H. Hosono, *Nat. Commun.*, 2013, **4**, 2378.
21 L. Liu, C. Zhao and Y. Li, *J. Phys. Chem. C*, 2012, **116(14)**, 7904-7912.
22 R. P. Ye, J. Ding, W. Gong, M. D. Argyle, Q. Zhong, Y. Wang, C. K. Russell, Z. Xu, A. G. Russell, Q. Li, M. Fan and Y. Yao, *Nat. Commun.* 2019, **10**, 5698.